Nano Res. 2012, 5(2): 109–116
DOI 10.1007/s12274-011-0190-1
Research Article

ISSN 1998-0124
CN 11-5974/O4

Functionalization of Silicon Nanowire Surfaces with Metal–Organic Frameworks

Nian Liu[1], Yan Yao[2], Judy J. Cha[2], Matthew T. McDowell[2], Yu Han[3], and Yi Cui[2,4] (✉)

[1] Department of Chemistry, Stanford University, Stanford, California 94305, USA
[2] Department of Materials Science and Engineering, Stanford University, Stanford, California 94305, USA
[3] Advanced Membrane and Porous Materials Center, King Abdullah University of Science and Technology, Thuwal 23955-6900, Saudi Arabia
[4] Stanford Institute for Materials and Energy Sciences, SLAC National Accelerator Laboratory, 2575 Sand Hill Road, Menlo Park, California 94025, USA

Received: 14 November 2011 / Accepted: 29 November 2011

ABSTRACT

Metal–organic frameworks (MOFs) and silicon nanowires (SiNWs) have been extensively studied due to their unique properties; MOFs have high porosity and specific surface area with well-defined nanoporous structure, while SiNWs have valuable one-dimensional electronic properties. Integration of the two materials into one composite could synergistically combine the advantages of both materials and lead to new applications. We report the first example of a MOF synthesized on surface-modified SiNWs. The synthesis of polycrystalline MOF-199 (also known as HKUST-1) on SiNWs was performed at room temperature using a step-by-step (SBS) approach, and X-ray photoelectron spectroscopy, X-ray diffraction, scanning electron microscopy, transmission electron microscopy, and energy dispersive spectroscopy elemental mapping were used to characterize the material. Matching of the SiNW surface functional groups with the MOF organic linker coordinating groups was found to be critical for the growth. Additionally, the MOF morphology can by tuned by changing the soaking time, synthesis temperature and precursor solution concentration. This SiNW/MOF hybrid structure opens new avenues for rational design of materials with novel functionalities.

KEYWORDS

Silicon nanowire, metal-organic framework, step-by-step, surface modification, nanocomposite

1. Introduction

Metal–organic frameworks (MOFs) are porous crystalline materials in which metal ions are joined by organic linkers [1–4]. Due to their unique characteristics, such as high surface area and ordered micropores/mesopores, MOFs have a wide range of applications in gas storage [5–8], gas separation [9, 10], catalysis [11], ion/molecule sensing [12, 13], and drug delivery [14, 15]. The functionality of MOFs can easily be tuned by changing the organic/inorganic components or by post-modification [16]. However, MOFs are usually insulating, which is a limiting factor for their application [17]. Hence, complexing high surface area MOFs with other conducting/semiconducting materials would open doors to new applications not possible

Address correspondence to yicui@stanford.edu

before. Nanowires, particularly silicon nanowires (SiNWs), with their unique one-dimensional (1D) structure and controllable properties, have been studied for a decade and have attracted a great deal of interest with applications including transistors [18], nanosensors [19], solar cells [20], lithium ion batteries [21], and thermoelectric devices [22]. Integrating the one-dimensionality and electronic properties of SiNWs with the high surface area and porosity of MOFs would combine the unique properties of both materials and lead to novel applications.

In this study, we demonstrate for the first time a general approach to functionalize SiNWs with MOFs. To achieve uniform MOF deposition on SiNWs, a method that allows nanoscale thickness control is desirable. Conventional solvothermal synthesis usually produces bulk crystals of MOFs [23, 24]. Recently, a step-by-step (SBS) method was reported for synthesis of uniform thin films of MOFs with controllable thickness on both flat and nonstandard substrates [25–30]. Here we apply this SBS method to synthesize MOF-199 on SiNWs. MOF-199 (also known as HKUST-1 and $Cu_3(btc)_2$, btc = 1,3,5-benzenetricarboxylate) is chosen because it is a well-studied benchmark MOF [23] and it has vacant coordination sites at Cu centers for selective gas absorption [31]. Our fabrication steps are illustrated in Fig. 1. First, single crystalline SiNWs were grown on a Si(100) wafer using the Au-catalyzed vapor–liquid–solid process [32–37]. Oxygen plasma treatment was applied to clean the NW surface and to form a thin layer of SiO_2. Then, SiNWs were treated with (3-cyanopropyl)trichlorosilane to form cyano groups on the surface, which were further converted to carboxyl groups by concentrated sulfuric acid

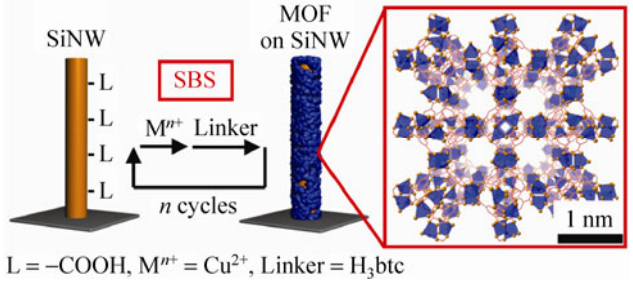

Figure 1 Schematic illustration of the synthesis of MOF-199 on SiNWs by using step-by-step (SBS) growth. On the right is the structure of MOF-199 (excluding guest species) viewed along the [100] direction

treatment [38]. Last, the SiNWs modified with carboxyl groups (Fig. 1, left) were alternately soaked in an ethanol solution of copper(Ⅱ) acetate ($Cu(OAc)_2$) and another ethanol solution of 1,3,5-benzenetricarboxylic acid (H_3btc) for 40 cycles. Each soaking lasts for 20 s. After each soaking, the sample was washed with ethanol to remove the excess reactant on the surface. In this way, MOF-199 can be successfully grown on SiNWs (Fig. 1, right).

2. Experimental

2.1 Synthesis and surface modification of SiNWs

SiNWs were grown inside a tube furnace using the vapor–liquid–solid method. First, a Si(100) wafer was covered by a 50 nm evaporated Au film as catalyst. The substrate was heated to 485 ℃ and silane (SiH_4, 2% in Ar) was flowed in at 80 sccm with a total chamber pressure of 30 Torr. The growth time was 20 min. The resulting SiNWs were treated with oxygen plasma for 5 min to produce a thin layer of SiO_2 on the SiNWs. To modify the SiNW surfaces with cyano groups, they were immersed in an anhydrous toluene solution of (3-cyanopropyl)trichlorosilane (1%) in an Ar-filled glovebox for 12 h, followed by rinsing in anhydrous toluene and ethanol. The –CN-modified SiNWs were hydrolyzed by heating in 50% (*v*/*v*) aqueous sulfuric acid at 150 ℃ for 3 h to obtain –COOH-modified SiNWs.

2.2 Step-by-step (SBS) growth of MOF-199 on SiNWs

Unless otherwise specified, –COOH-modified SiNWs were alternately soaked in a 10 mmol/L copper(Ⅱ) acetate ($Cu(OAc)_2$) ethanol solution and a 50 mmol/L H_3btc ethanol solution at room temperature for 10, 20, or 40 cycles. Each soaking lasted for 20 s. After each soaking, the sample was washed with ethanol to remove the excess reactant from the surface. For surface comparison experiments, SBS growth of MOF-199 on unmodified SiNWs was carried out in the same way.

2.3 Characterization of MOF-199 on SiNWs

Characterization was done using X-ray photoelectron spectroscopy (XPS, SSI S-Probe, monochromatized Al

Kα radiation at 1486 eV), X-ray diffraction (PANalytical X'Pert PRO, Ni-filtered Cu Kα radiation), scanning electron microscopy (FEI Sirion), and transmission electron microscopy (FEI Tecnai G2 F20 X-twin with an energy dispersive spectroscopy (EDS) X-ray detector). To form EDS elemental maps, 40 × 80 pixel spectra with an acquisition time of 500 ms per pixel were acquired in scanning TEM (STEM) mode.

3. Results and discussion

The growth of MOF-199 on SiNWs is reflected by the color change of the sample. As shown in Fig. S-1 in the Electronic Supplementary Material (ESM), as-synthesized SiNWs are brown, while MOF-199 powders are blue due to the presence of coordinated copper ions in the framework. With increasing number of SBS growth cycles, the color of the SiNWs became more blue, indicating the growth of the MOF on the SiNWs (Fig. S-1 in the ESM). Apart from the color changes, the surface characteristics of the SiNWs should also change after MOF growth. X-ray photoelectron spectroscopy (XPS) analysis was therefore carried out. The major surface elements on as-synthesized SiNWs are silicon and oxygen (Fig. 2, orange line) from the native surface oxide. After MOF growth, the carbon 1s and oxygen 1s peaks increase in intensity while the silicon peaks decrease in intensity (Fig. 2, blue line). The Cu $2p_{3/2}$ peak, which originates from the Cu in MOF-199, is clearly visible after the growth process. Therefore, the surfaces of the SiNWs are terminated by MOF components (either organic linker or Cu). Since XPS has an analysis depth of 1–5 nm, which is beyond the size of one btc linker (< 1 nm), we cannot determine whether Cu ions or organic linkers are present at the outer surface layer. However, the SBS growth ends with soaking in H_3btc solution, so it is expected that the organic linkers terminate the MOF at the outer surface.

The X-ray diffraction (XRD) pattern of MOF-199 on SiNWs was essentially identical to that of MOF-199 powder synthesized according to the literature [24], confirming the growth of crystalline MOF-199 on SiNWs (Fig. 3). All the MOF peaks are present in the diffraction pattern of SiNW/MOF sample. Apart from the peaks produced by MOF-199, one more peak at

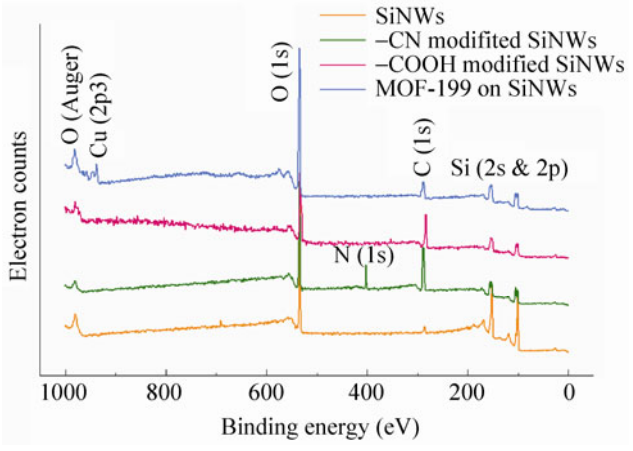

Figure 2 X-ray photoelectron spectroscopy (XPS) results from pristine SiNWs, –CN modified SiNWs, –COOH modified SiNWs, and MOF-199 grown on SiNWs. All the spectra were collected under the same conditions without further processing

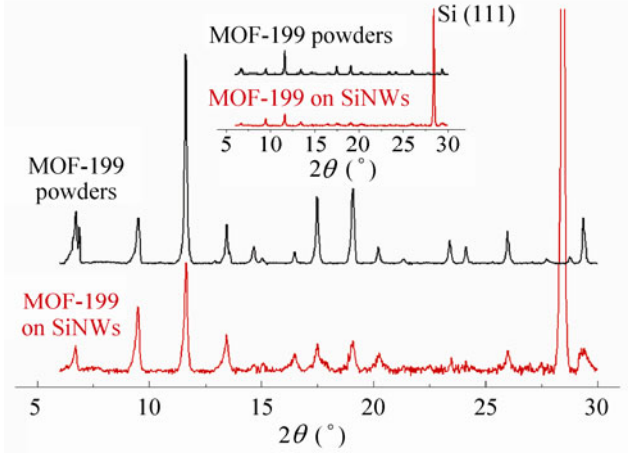

Figure 3 XRD patterns of the as-synthesized MOF-199 grown on SiNWs and the MOF-199 powder synthesized according to Ref. [24]. The Si(111) peak is truncated to show the peaks from MOF-199. Complete patterns are shown in the inset

the 2θ value of 28.4° can be indexed to Si(111). This peak is from the SiNWs, because the substrate is a (100)-oriented silicon wafer.

Scanning electron microscopy (SEM) images show that as-synthesized SiNWs have smooth surfaces and have an Au catalyst particle on the tips (Fig. 4(a)). After 40 cycles of SBS growth, the surfaces become rough due to the growth of MOF-199 on the SiNWs (Fig. 4(b)). The MOF grown on SiNWs has a much smaller domain size than that in the powder form (usually micron-sized). The smaller crystal size is due to the step-by-step (or layer-by-layer) nature of the crystal

growth mechanism. Ideally, each crystal grows by one layer of molecular building blocks in each step, allowing the crystal size to be controlled within the range of several or several tens of nanometers [39], which allows for more precise size control than for the MOF powder obtained using the conventional solvothermal method. It is also noted from the SEM images that the MOF almost covers the whole NW surface area, including the tips where the Au catalyst particles are located. This conformal growth can also be attributed to the SBS growth. Because the two building blocks, $Cu(OAc)_2$ and H_3btc, are supplied in two separate steps, the nucleation and crystal growth of MOF only happen at the SiNW surfaces. Given the smooth surfaces of SiNWs and the conformal –COOH modification, the MOF will cover the whole NW surface area. Therefore, this SBS growth mechanism is ideal for the nanoscale functionalization of SiNWs with MOFs. To study the morphology evolution during SBS growth of MOF-199 on SiNWs, SEM images were taken after 0, 10, 20, and 40 growth cycles (Fig. S-2 in the ESM). After 10 SBS cycles, the nucleation of MOF crystals is evident at discrete locations on the NW surfaces. With more growth cycles, both the number and size of the MOF nanocrystals increases. After 40 cycles, a uniform MOF-199 coating covers the whole surface of the SiNWs. The thickness of the MOF shell can be tailored by controlling the number of cycles.

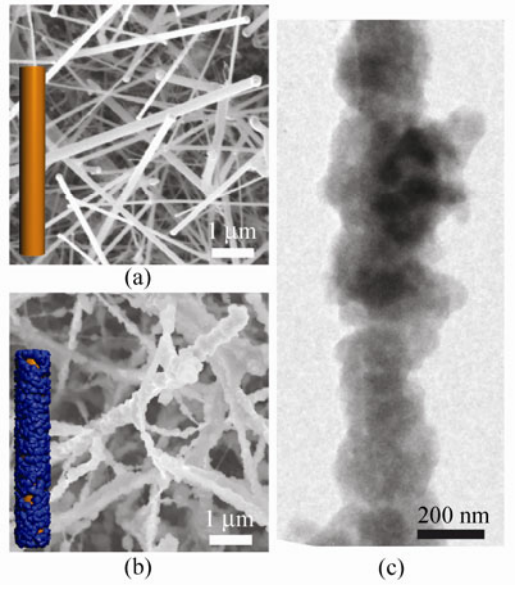

Figure 4 SEM images of (a) as-grown SiNWs and (b) MOF-199-coated SiNWs after 40 cycles of SBS growth; (c) TEM image of MOF-199-coated SiNWs after 40 cycles of SBS growth

The structure of MOF-199 on SiNWs was studied by transmission electron microscopy (TEM). After 40 cycles of SBS growth, SiNW/MOF-199 hybrid was detached from the substrate and attached to a TEM grid. As shown in Fig. 4(c), the SiNW core in the middle has slightly higher contrast than the MOF shell. The lower contrast of MOF-199 could be caused by its high porosity (the void fraction is 0.41 according to Ref. [23]) and organic components. MOF-199 has a density of 1.22 g/cm^3 [23], only about half of the density of crystalline Si (2.33 g/cm^3). It is also shown in Fig. 4(c) that the MOF conformally coats the SiNWs and causes moderate surface roughness. The thickness of the MOF shell is about 80–120 nm after 40 cycles of SBS growth. On average, the thickness increases by 2–3 nm every cycle, which is on the order of unit cell dimension (2.6 nm) [23]. This result suggests that the MOF shell grows by a layer-by-layer mechanism. Additionally, the MOF grown on SiNWs is not as smooth as that grown on flat substrate. Furthermore the obtained MOF is polycrystalline. This could be due to the nanoscale curvature of the SiNW surfaces, which prevents the formation of single-crystalline films.

Energy dispersive spectroscopy (EDS) elemental mapping was carried out to study the spatial distribution of Si (from the SiNWs) and Cu (from the MOF-199) (Fig. 5). Nickel TEM grids were used so that the Cu signal arose only from the MOF-199. The Si elemental signal is spatially localized in the core with a sharp boundary at the edge of the NW, which confirms that the SiNW structure is not affected by the MOF-199 coating. The Cu signal from the MOF is dispersed primarily in the shell around the SiNW, which indicates a surface coating of MOF-199 on the SiNWs.

Matching the surface functional groups on the SiNW surface with the organic linker of the MOF in the synthesis is the critical step leading to strong chemical bonding and therefore a high quality coating of MOF on SiNWs. XPS was used to characterize the surface of the SiNWs after every step of the surface modification process (Fig. 2). The simultaneous appearance of the N(1s) and C(1s) peaks (green spectrum) indicates the

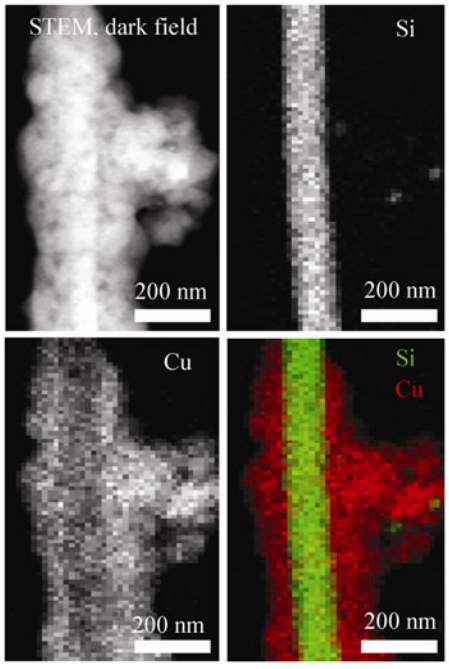

Figure 5 Dark-field scanning transmission electron microscopy (STEM) image and energy dispersive spectroscopy (EDS) elemental mapping of MOF-199 on a SiNW indicating the spatial elemental distribution of silicon and copper. The copper signal is from MOF-199

presence of the cyano groups on the SiNWs, while the disappearance of the N(1s) peak and the preservation of the C(1s) peak after sulfuric acid treatment (pink spectrum) indicates the conversion of the cyano groups to carboxyl groups. For comparison, SBS growth of MOF-199 was performed on SiNWs without surface modification (SiNWs with native oxide). A SEM image (Fig. 6) shows that MOF-199 aggregates and forms non-uniform coatings on unmodified SiNWs, even after 60 cycles of SBS growth. In addition, the growth of MOF-199 occurs much more slowly on native oxide-covered SiNWs (Fig. S-3 in the ESM) than on –COOH-modified SiNWs (Fig. S-2 in the ESM). These observations show that the –COOH modification of SiNWs is crucial for the successful growth of MOF-199 on SiNWs. Similar effects have been reported for the growth of MOF-5 on flat silica substrates and the growth of MIL-47 on polyacrylonitrile substrates [40, 41]. Adopting this general guideline, the SBS growth of MOF-199 on SiNWs could be extended to a broader choice of coordination polymers on NWs. For example, zeolitic imidazolate frameworks (ZIFs) [42–44]) on $–NH_2$-modified SiNWs can be anticipated.

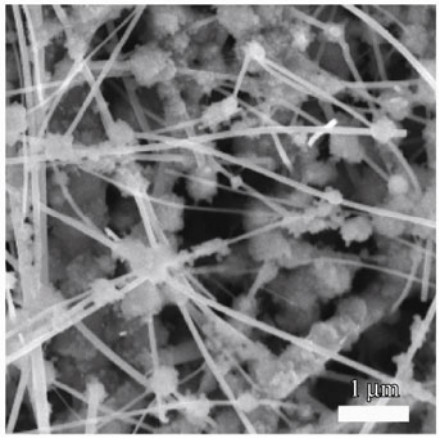

Figure 6 SEM image of MOF-199 grown on unmodified SiNWs with 60 cycles of SBS growth. The SiNWs had no –COOH modification and only had native oxide on their surfaces. MOF-199 grew slowly and formed non-uniform coatings on these unmodified SiNWs

The effect of varying the solution concentration, immersion time and growth temperature on the morphology of MOF-199 grown on SiNWs was also studied. First, the $Cu(OAc)_2$ solution concentration was reduced from 10 mmol/L to 1 mmol/L and the H_3btc solution concentration was reduced from 50 mmol/L to 0.1 mmol/L. At the same time, the immersion time was increased from 20 s to 30 min in $Cu(OAc)_2$ and 60 min in H_3btc. Under these conditions, 30–50 nm bud-like domains of MOF-199 are obtained on SiNWs with high coverage after 10 growth cycles (Figs. 7(a) and 7(b)). It is clear that longer immersion times allow the MOF-199 crystal to grow larger. This may be due to Ostwald ripening during the SBS growth of the MOF-199 [45]. Next, the SBS growth temperature was increased from 25 ℃ to 60 ℃ while keeping the low concentrations (0.1 and 1 mmol/L) and long immersion times (30 and 60 min for each solution, respectively). Interestingly, the resulting MOF-199 (Figs. 7(c), 7(d) and Fig. S-4 in the ESM) has smaller domain size and similar morphology to that synthesized at 25 ℃ with higher solution concentrations (10 and 50 mmol/L) and shorter immersion times (20 s), as shown in Figs. 4(b) and 4(c). The higher nucleation rate at higher temperature may be the reason for the small domain size [46]. These experiments show that the morphology of the MOF-199 grown on SiNWs can easily be tuned by adjusting the solution concentration, immersion time and growth temperature.

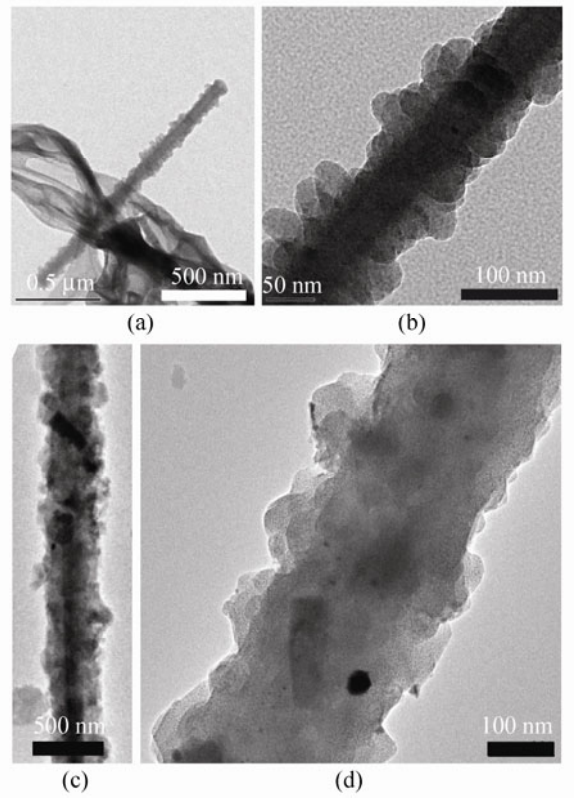

Figure 7 (a, b) TEM images of MOF-199 grown on SiNWs at 25 ˚C with 10 cycles of SBS growth. SiNWs on a substrate were alternately immersed in a 1 mmol/L $Cu(OAc)_2$ ethanol solution for 30 min and a 0.1 mmol/L H_3btc ethanol solution for 60 min. (c, d) TEM images of MOF-199 grown on SiNWs at 60 ˚C with 10 cycles of SBS growth. The SiNWs were alternatively immersed in a 1 mmol/L $Cu(OAc)_2$ ethanol solution for 30 min and a 0.1 mmol/L H_3btc ethanol solution for 60 min

4. Conclusions

For the first time, we have demonstrated that a metal–organic framework can be grown on the surface of SiNWs by a step-by-step growth mechanism. This mechanism allows controllable and conformal growth of MOFs at the nanometer scale. The MOF-199 grown on SiNWs is polycrystalline with good surface coverage. We have found that the matching of the SiNW surface groups and the MOF coordinating groups is crucial for the successful growth of MOFs on SiNWs. In addition, the morphology of MOF grown on the SiNWs has been found to depend on the solution concentration, immersion time, and growth temperature. Given the flexible methods for the chemical modification of SiNW surfaces, the growth of a wide range of MOFs and ZIFs on SiNWs is anticipated. The hybridization of these two kinds of unique materials opens doors for exciting new applications combining the advantageous properties of both materials.

Acknowledgements

YC acknowledges the support from ONR and KAUST Investigator Award (NO. KUS-l1-01-12). A portion of this work was supported by the Department of Energy, Office of Basic Energy Sciences, Division of Materials Sciences and Engineering under contract DE-AC02-76SF00515 through the SLAC National Accelerator Laboratory LDRD project. MTM acknowledges support from the Chevron Stanford Graduate Fellowship, the National Defense Science and Engineering Graduate Fellowship, and the National Science Foundation Graduate Fellowship.

Electronic Supplementary Material: Supplementary material (optical images of MOF-199 powders and MOF-199 on SiNWs; supplementary SEM and TEM images of MOF-199 on SiNWs with different synthesis conditions) is available in the online version of this article at http://dx.doi.org/10.1007/s12274-011-0190-1 and may be accessed free of charge.

References

[1] Li, H.; Eddaoudi, M.; O'Keeffe, M.; Yaghi, O. M. Design and synthesis of an exceptionally stable and highly porous metal–organic framework. *Nature* **1999**, *402*, 276–279.

[2] Eddaoudi, M.; Moler, D. B.; Li, H. L.; Chen, B. L.; Reineke, T. M.; O'Keeffe, M.; Yaghi, O. M. Modular chemistry: Secondary building units as a basis for the design of highly porous and robust metal–organic carboxylate frameworks. *Acc. Chem. Res.* **2001**, *34*, 319–330.

[3] Yaghi, O. M.; O'Keeffe, M.; Ockwig, N. W.; Chae, H. K.; Eddaoudi, M.; Kim, J. Reticular synthesis and the design of new materials. *Nature* **2003**, *423*, 705–714.

[4] Kitagawa, S.; Kitaura, R.; Noro, S. Functional porous coordination polymers. *Angew. Chem. Int. Ed.* **2004**, *43*, 2334–2375.

[5] Eddaoudi, M.; Kim, J.; Rosi, N.; Vodak, D.; Wachter, J.; O'Keeffe, M.; Yaghi, O. M. Systematic design of pore size and functionality in isoreticular MOFs and their application in methane storage. *Science* **2002**, *295*, 469–472.

[6] Rosi, N. L.; Eckert, J.; Eddaoudi, M.; Vodak, D. T.; Kim, J.; O'Keeffe, M.; Yaghi, O. M. Hydrogen storage in microporous metal–organic frameworks. *Science* **2003**, *300*, 1127–1129.

[7] Millward, A. R.; Yaghi, O. M. Metal–organic frameworks with exceptionally high capacity for storage of carbon dioxide at room temperature. *J. Am. Chem. Soc.* **2005**, *127*, 17998–17999.

[8] Murray, L. J.; Dinca, M.; Long, J. R. Hydrogen storage in metal–organic frameworks. *Chem. Soc. Rev.* **2009**, *38*, 1294–1314.

[9] Chen, B. L.; Liang, C. D.; Yang, J.; Contreras, D. S.; Clancy, Y. L.; Lobkovsky, E. B.; Yaghi, O. M.; Dai, S. A Microporous metal–organic framework for gas-chromatographic separation of alkanes. *Angew. Chem. Int. Ed.* **2006**, *45*, 1390–1393.

[10] Li, J. R.; Kuppler, R. J.; Zhou, H. C. Selective Gas Adsorption and separation in metal–organic frameworks. *Chem. Soc. Rev.* **2009**, *38*, 1477–1504.

[11] Seo, J. S.; Whang, D.; Lee, H.; Jun, S. I.; Oh, J.; Jeon, Y. J.; Kim, K. A homochiral metal–organic porous material for enantioselective separation and catalysis. *Nature* **2000**, *404*, 982–986.

[12] Kreno, L. E.; Hupp, J. T.; Van Duyne, R. P. Metal–organic framework thin film for enhanced localized surface plasmon resonance gas sensing. *Anal. Chem.* **2010**, *82*, 8042–8046.

[13] Lu, G.; Hupp, J. T. Metal–organic frameworks as sensors: A ZIF-8 based Fabry–Perot device as a selective sensor for chemical vapors and gases. *J. Am. Chem. Soc.* **2010**, *132*, 7832–7833.

[14] Horcajada, P.; Serre, C.; Maurin, G.; Ramsahye, N. A.; Balas, F.; Vallet-Regi, M.; Sebban, M.; Taulelle, F.; Ferey, G. Flexible porous metal–organic frameworks for a controlled drug delivery. *J. Am. Chem. Soc.* **2008**, *130*, 6774–6780.

[15] Della Rocca, J.; Liu, D. M.; Lin, W. B. Nanoscale metal–organic frameworks for biomedical imaging and drug delivery. *Acc. Chem. Res.* **2011**, *44*, 957–968.

[16] Chae, H. K.; Siberio-Perez, D. Y.; Kim, J.; Go, Y.; Eddaoudi, M.; O'Keeffe, M.; Yaghi, O. M.; Matzger, A. J. A Route to high surface area, porosity and inclusion of large molecules in crystals. *Nature* **2004**, *427*, 523–527.

[17] Jahan, M.; Bao, Q. L.; Yang, J. X.; Loh, K. P. Structure-directing role of graphene in the synthesis of metal–organic framework nanowire. *J. Am. Chem. Soc.* **2010**, *132*, 14487–14495.

[18] Cui, Y.; Lieber, C. M. Functional nanoscale electronic devices assembled using silicon nanowire building blocks. *Science* **2001**, *291*, 851–853.

[19] Cui, Y.; Wei, Q. Q.; Park, H. K.; Lieber, C. M. Nanowire nanosensors for highly sensitive and selective detection of biological and chemical species. *Science* **2001**, *293*, 1289–1292.

[20] Tian, B. Z.; Zheng, X. L.; Kempa, T. J.; Fang, Y.; Yu, N. F.; Yu, G. H.; Huang, J. L.; Lieber, C. M. Coaxial silicon nanowires as solar cells and nanoelectronic power sources. *Nature* **2007**, *449*, 885–889.

[21] Chan, C. K.; Peng, H. L.; Liu, G.; McIlwrath, K.; Zhang, X. F.; Huggins, R. A.; Cui, Y. High-performance lithium battery anodes using silicon nanowires. *Nat. Nanotechnol.* **2008**, *3*, 31–35.

[22] Hochbaum, A. I.; Chen, R. K.; Delgado, R. D.; Liang, W. J.; Garnett, E. C.; Najarian, M.; Majumdar, A.; Yang, P. D. Enhanced thermoelectric performance of rough silicon nanowires. *Nature* **2008**, *451*, 163–167.

[23] Chui, S. S. Y.; Lo, S. M. F.; Charmant, J. P. H.; Orpen, A. G.; Williams, I. D. A chemically functionalizable nanoporous material $[Cu_3(TMA)_2(H_2O)_3]_n$. *Science* **1999**, *283*, 1148–1150.

[24] Rowsell, J. L. C.; Yaghi, O. M. Effects of functionalization, catenation, and variation of the metal oxide and organic linking units on the low-pressure hydrogen adsorption properties of metal–organic frameworks. *J. Am. Chem. Soc.* **2006**, *128*, 1304–1315.

[25] Shekhah, O.; Wang, H.; Kowarik, S.; Schreiber, F.; Paulus, M.; Tolan, M.; Sternemann, C.; Evers, F.; Zacher, D.; Fischer, R. A.; Woll, C. Step-by-step route for the synthesis of metal–organic frameworks. *J. Am. Chem. Soc.* **2007**, *129*, 15118–15119.

[26] Shekhah, O.; Wang, H.; Zacher, D.; Fischer, R. A.; Woll, C. Growth mechanism of metal–organic frameworks: Insights into the nucleation by employing a step-by-step route. *Angew. Chem. Int. Ed.* **2009**, *48*, 5038–5041.

[27] Bétard, A. l.; Fischer, R. A. Metal–organic framework thin films: From fundamentals to applications. *Chem. Rev.,* in press, DOI: 10.1021/cr200167v.

[28] Biemmi, E.; Darga, A.; Stock, N.; Bein, T. Direct growth of $Cu_3(btc)_2(H_2O)_3{\cdot}xH_2O$ thin films on modified QCM–gold electrodes–water sorption isotherms. *Micropor. Mesopor. Mat.* **2008**, *114*, 380–386.

[29] Lu, G.; Farha, O. K.; Kreno, L. E.; Schoenecker, P. M.; Walton, K. S.; Van Duyne, R. P.; Hupp, J. T. Fabrication of metal–organic framework-containing silica-colloidal crystals for vapor sensing. *Adv. Mater.* **2011**, *23*, 4449–4452.

[30] Arslan, H. K.; Shekhah, O.; Wohlgemuth, J.; Franzreb, M.; Fischer, R. A.; Wöll, C. High-throughput fabrication of uniform and homogenous MOF coatings. *Adv. Funct. Mater.* **2011**, *21*, 4228–4231.

[31] Britt, D.; Tranchemontagne, D.; Yaghi, O. M. Metal–organic frameworks with high capacity and selectivity for harmful gases. *Proc. Natl. Acad. Sci USA* **2008**, *105*, 11623–11627.

[32] Morales, A. M.; Lieber, C. M. A laser ablation method for the synthesis of crystalline semiconductor nanowires. *Science* **1998**, *279*, 208–211.

[33] Huang, M. H.; Wu, Y. Y.; Feick, H.; Tran, N.; Weber, E.; Yang, P. D. Catalytic growth of zinc oxide nanowires by vapor transport. *Adv. Mater.* **2001**, *13*, 113–116.

[34] Pan, Z. W.; Dai, Z. R.; Wang, Z. L. Nanobelts of semiconducting oxides. *Science* **2001**, *291*, 1947–1949.

[35] Dick, K. A.; Deppert, K.; Karlsson, L. S.; Wallenberg, L. R.; Samuelson, L.; Seifert, W. A new understanding of Au-assisted growth of Ⅲ–Ⅴ semiconductor nanowires. *Adv. Funct. Mater.* **2005**, *15*, 1603–1610.

[36] Hannon, J. B.; Kodambaka, S.; Ross, F. M.; Tromp, R. M. The influence of the surface migration of gold on the growth of silicon nanowires. *Nature* **2006**, *440*, 69–71.

[37] Wang, Y. W.; Schmidt, V.; Senz, S.; Gosele, U. Epitaxial growth of silicon nanowires using an aluminium catalyst. *Nat. Nanotechnol.* **2006**, *1*, 186–189.

[38] Karimi, B.; Zamani, A.; Abedia, S.; Clark, J. H. Aerobic oxidation of alcohols using various types of immobilized palladium catalyst: The synergistic role of functionalized ligands, morphology of support, and solvent in generating and stabilizing nanoparticles. *Green Chem.* **2009**, *11*, 109–119.

[39] Zacher, D.; Schmid, R.; Woll, C.; Fischer, R. A. Surface chemistry of metal–organic frameworks at the liquid–solid interface. *Angew. Chem. Int. Ed.* **2011**, *50*, 176–199.

[40] Hermes, S.; Zacher, D.; Baunemann, A.; Woll, C.; Fischer, R. A. Selective growth and MOCVD loading of small single crystals of MOF-5 at alumina and silica surfaces modified with organic self-assembled monolayers. *Chem. Mater.* **2007**, *19*, 2168–2173.

[41] Centrone, A.; Yang, Y.; Speakman, S.; Bromberg, L.; Rutledge, G. C.; Hatton, T. A. Growth of metal–organic frameworks on polymer surfaces. *J. Am. Chem. Soc.* **2010**, *132*, 15687–15691.

[42] Park, K. S.; Ni, Z.; Cote, A. P.; Choi, J. Y.; Huang, R. D.; Uribe-Romo, F. J.; Chae, H. K.; O'Keeffe, M.; Yaghi, O. M. Exceptional chemical and thermal stability of zeolitic imidazolate frameworks. *Proc. Natl. Acad. Sci. USA* **2006**, *103*, 10186–10191.

[43] Wang, B.; Cote, A. P.; Furukawa, H.; O'Keeffe, M.; Yaghi, O. M. Colossal cages in zeolitic imidazolate frameworks as selective carbon dioxide reservoirs. *Nature* **2008**, *453*, 207–211.

[44] Phan, A.; Doonan, C. J.; Uribe-Romo, F. J.; Knobler, C. B.; O'Keeffe, M.; Yaghi, O. M. Synthesis, structure, and carbon dioxide capture properties of zeolitic imidazolate frameworks. *Acc. Chem. Res.* **2010**, *43*, 58–67.

[45] Zacher, D.; Liu, J. N.; Huber, K.; Fischer, R. A. Nanocrystals of $[Cu_3(btc)_2]$ (HKUST-1): A combined time-resolved light scattering and scanning electron microscopy study. *Chem. Commun.* **2009**, 1031–1033.

[46] Millange, F.; Medina, M. I.; Guillou, N.; Ferey, G.; Golden, K. M.; Walton, R. I. Time-resolved *in situ* diffraction study of the solvothermal crystallization of some prototypical metal–organic frameworks. *Angew. Chem. Int. Ed.* **2010**, *49*, 763–766.